High-pressure X-ray diffraction study and equation of state of MgSiO₃ ilmenite

Bruno Reynard,[1] Guillaume Fiquet,[2] Jean-Paul Itié,[3] and David C. Rubie[4]

[1] Laboratoire de Minéralogie Physique, Géosciences Rennes, UPR CNRS 4661, 35042 Rennes Cedex, France
[2] Laboratoire des Sciences de la Terre, URA CNRS 726, Ecole Normale Supérieure,
46, Allée d'Italie, 69364 Lyon Cedex 07, France
[3] Laboratoire des Milieus Condensés, URA CNRS 782, Université Pierre et Marie Curie,
4, Place Jussieu, 75252 Paris Cedex 05, France
[4] Bayerisches Geoinstitut, Universität Bayreuth, D-95440 Bayreuth, Germany

ABSTRACT

High-pressure X-ray powder diffraction data for MgSiO₃ ilmenite have been collected up to 28 GPa using a diamond-anvil cell in an energy-dispersive configuration at the storage ring DCI at the LURE (Orsay, France). H₂O was used as a pressure-transmitting medium. Pressures were measured using the ruby-fluorescence method or estimated from the equation of state of ice VII. Both pressure determinations are in good agreement up to 15 GPa but diverge at higher pressures because of the development of nonhydrostatic stresses and pressure gradients marked by an increase of the ruby-fluorescence line width. No phase changes are observed during compression or decompression. The compression of MgSiO₃ ilmenite is anisotropic, with the c axis being twice as compressible as the a axis. The high-pressure volume data were fitted to a third-order Birch-Murnaghan equation of state and are consistent with the former determination of $K_0 = 212$ GPa by Brillouin scattering; the data yield $K_0' = 7.5(10)$ if the ruby-fluorescence pressures are used or $K_0' = 5.6(10)$ if the pressures obtained from the equation of state of ice VII are used; the latter value is preferred because pressures were determined on the X-ray spot. The effects of nonhydrostatic stresses and pressure gradients on the determination of equations of state are discussed.

INTRODUCTION

MgSiO₃ ilmenite is a high-pressure polymorph of enstatite that is characterized by a relatively narrow stability field in the 20–24 GPa range, bounded at low pressures by the β- or γ-Mg₂SiO₄ + stishovite assemblage stability field, at high pressures and temperatures by the MgSiO₃ perovskite stability field, and, marginally, at high temperatures (>2200 K) by the majorite stability field (Ito and Matsui 1977; Ito and Yamada 1982; Ito and Navrotsky 1985; Sawamoto 1987). Because of its stability at relatively low temperatures, it is potentially an important constituent of subducting slabs in the 600–700 km depth range in the Earth's mantle. At low temperatures in subducting lithosphere, clinoenstatite may persist metastably in the β-Mg₂SiO₄ + stishovite stability field before transforming directly to ilmenite (Hogrefe et al. 1994). Because of its large volume change, this metastable clinoenstatite-to-ilmenite transformation is likely to affect stresses and buoyancy forces in the slab and may also be related to the mechanisms of deep-focus earthquakes. Finally, the stability of ilmenite extends a few tens of kilometers into the lower mantle at low temperatures, so that the presence of this phase may cause a negative density anomaly within the surrounding mantle where perovskite is stable, thus inhibiting slab penetra-

tion into the lower mantle. The modeling of such anomalies and a detailed refinement of thermodynamic properties of high-pressure phases in the MgSiO₃-Mg₂SiO₄ system (Ashida et al. 1988; Fei et al. 1990; Gasparik 1990) require a precise knowledge of the equation of state (EOS) of MgSiO₃ ilmenite. To date, only its ambient pressure bulk modulus has been determined by Brillouin scattering (Weidner and Ito 1985). Thus, we have performed a high-pressure powder X-ray diffraction study of MgSiO₃ ilmenite at pressures up to its stability field using synchrotron radiation.

EXPERIMENTAL METHODS

Sample synthesis

Powders of dry MgSiO₃ glass synthesized by Neuville and Richet (1991) were used as a starting material and transformed to ilmenite at 22.5 GPa and 1200 °C for 2.5 h using the 1200 ton multi-anvil press at the Bayerisches Geoinstitut. The sample was confirmed by both X-ray powder diffraction and Raman spectroscopy to be pure ilmenite phase. Least-squares refinement of the ambient lattice parameters from the X-ray diffraction data gave $a = 4.722(2)$ and $c = 13.560(12)$ Å, in good agreement with previous determinations (e.g., Ito and Matsui 1977), and Raman frequencies are consistent with those given by

TABLE 1. Unit-cell parameters of MgSiO$_3$ ilmenite as a function of pressure

P_r (GPa)	P_i (GPa)	a (Å)	c (Å)	V (Å^3)	n	V_{ice} (Å^3)
0.00		4.7273(23)	13.546(12)	262.17(49)	6*	
0.95[5]		4.7240(40)	13.491(23)	260.49(89)	7**	
2.40[5]	2.35[3]	4.7115(11)	13.489(7)	259.32(26)	7**	11.32(14)
4.25[10]	n.d.	4.7035(17)	13.449(12)	257.67(42)	8	n.d.
6.1[1]	5.8[1]	4.6951(16)	13.401(11)	255.83(38)	8	10.37(14)
9.1[1]	8.6[2]	4.6826(20)	13.324(13)	253.01(46)	8	9.81(13)
10.9[1]	10.3[2]	4.6746(33)	13.274(21)	251.20(75)	8	9.52(13)
13.0[2]	12.4[4]	4.6643(52)	13.227(31)	249.21(114)	8	9.22(13)
15.5[2]	15.0[6]	4.6533(42)	13.215(28)	247.81(97)	8	8.91(12)
17.8[2]	16.3[5]	4.6508(21)	13.139(14)	246.12(48)	8	8.77(12)
20.7[4]	19.0[7]	4.6358(32)	13.083(21)	243.49(73)	8	8.50(12)
24.5[5]	22.2[11]	4.6256(24)	12.988(14)	240.66(51)	8	8.22(12)
27.8[5]	25.2[14]	4.6190(29)	12.942(20)	239.13(67)	7†	8.00(11)
20.4[5]	21.4[13]	4.6354(24)	13.021(15)	242.30(53)	7†	8.26(12)
10.1[3]	12.1[8]	4.6830(51)	13.256(28)	251.76(108)	7‡	9.23(13)
0.00		4.7308(14)	13.541(9)	262.45(33)	8	

Note: Estimated standard deviations (1σ) in parentheses for cell parameters. P_r is the pressure determined from the ruby-fluorescence method (uncertainties in brackets from fluorescence line widths); P_i is the pressure determined from the ice-VII EOS (maximum pressure gradients in brackets, estimated from diffraction line widths); n is the number of reflections used in the refinement; parameters refined with the (012), (104), (110), (113), (024), (116), (214), and (030) reflections, unless specified; V_{ice} is the volume of ice VII obtained from the (110) line (uncertainties estimated from the standard errors on peak location are probably underestimated); n.d. = not determined.
 * The (214) and (030) reflections unobserved.
 ** The (110) reflection unobserved or interfered with ice reflection.
 † The (024) reflection unobserved.
 ‡ The (214) reflection unobserved.

McMillan and Ross (1987). Grain size is about 5–10 μm (optical observation).

High-pressure diffraction experiment

An 80 μm diameter chip of polycrystalline sample was loaded into the 200 μm hole of a 301 stainless steel gasket in a diamond cell equipped with 600 μm culet diamonds, along with two small (5–10 μm) ruby chips and pure H$_2$O as a pressure-transmitting medium. High-pressure powder X-ray measurements were conducted at ambient temperature in an energy-dispersive mode at the storage ring DCI (LURE, Orsay, France). The sample was X-rayed in the diamond-anvil cell by a polychromatic X-ray beam, collimated by a remote tungsten-carbide slit system to a 50 μm diameter spot centered on the pressure chamber. The diffracted beam was analyzed at 11.439° 2θ between 5 and 50 keV by a Canberra planar germanium detector (efficient area 50 mm²), with a resolution between 145 eV at 5.9 keV and 500 eV at 122 keV. We used a large sample-detector distance combined with a 100 μm detector-entrance slit and a 2θ defining slit system to record the patterns with a resolution close to the theoretical capabilities of the detector. Thin silver foil placed between the diamonds was used as a standard to calibrate the system in the operating geometry used for the high-pressure measurements on MgSiO$_3$ ilmenite.

Pressure measurements and pressure-gradient estimation

Pressure was monitored by the ruby-fluorescence method. Ruby-fluorescence line widths were used to detect nonhydrostatic conditions. Significant broadening did not occur up to 15 GPa, indicating quasi-hydrostatic behavior up to this pressure. Pressures were checked before and after each data collection and were found to be identical within experimental uncertainties, indicating that no pressure drop occurs in the diamond cell chamber within the typical duration of the X-ray data collection (30–45 min). Above 15 GPa, significant broadening of the ruby-fluorescence lines occurred and increased with increasing pressure. An independent check of the pressure measurements was provided by the use of H$_2$O as a pressure medium. Above 2.3 GPa, H$_2$O transforms to the ice-VII polymorph, which is stable throughout the pressure range investigated here (Hemley et al. 1987). We were able to follow the (110) line of ice VII and used the equation of state determined by Hemley et al. (1987) to recalculate pressures in our experiment (Table 1, Fig. 1). This procedure prevents any bias resulting from pressure gradients in the cell chamber because the X-ray measurements on ice and ilmenite were obtained from the same area. The two pressure determinations are in overall agreement up to 15 GPa, where discrepancies increase to reach 2.5 GPa at the maximum pressure of 27.8 GPa. In addition, a significant increase of the (110) line width of ice VII was observed with increasing pressure, from 120 eV at 2.4 GPa to 200 eV at the maximum pressure and to 240 eV upon decreasing pressure. If we assume that this broadening is due only to the pressure differences across the X-rayed spot, the pressure difference can be estimated from

$$\Delta P = \Delta E_{110}/(\partial E_{110}/\partial P) \qquad (1)$$

where ΔE_{110} is the line broadening with respect to the ambient pressure-extrapolated value (~100 eV) and $(\partial E_{110}/\partial P)$ is the slope of the energy variation of the ice-VII (110) line with pressure. The pressure differences are plotted in Figure 2a and reach 1.5 GPa at the maximum pressure. It is worth noticing that the differences are roughly correlated to the difference between the ruby- and
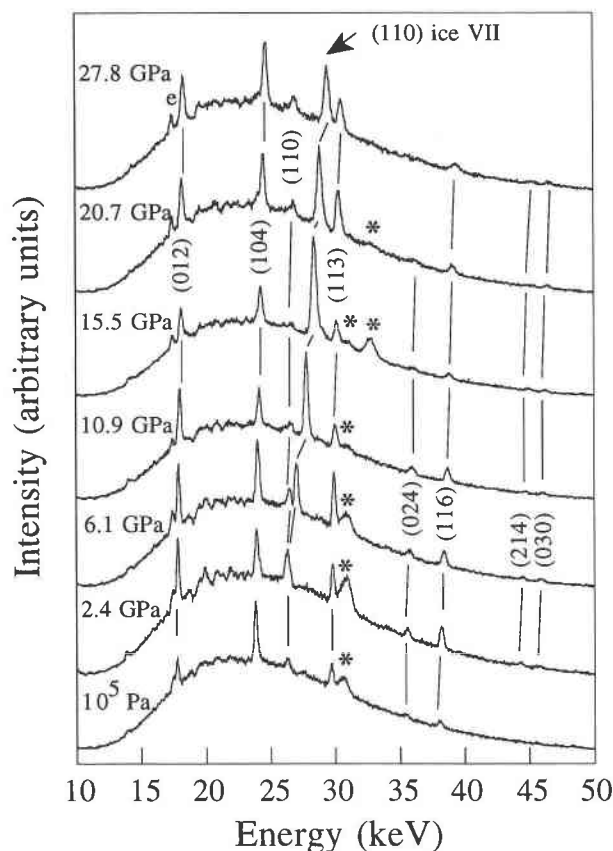
FIGURE 1. Evolution of the X-ray powder diffraction spectra with pressure. Notice the appearance of the ice-VII (110) peak at 2.4 GPa and the increase of its line width with increasing pressure. Peaks from MgSiO₃ ilmenite shown with the indexing used for the unit-cell parameter refinements. Asterisks mark peaks from the metallic gasket; e = escape peak.

FIGURE 2. (a) Pressure differences across the X-rayed spot calculated from the (110) ice-VII line-width increase using Eq. 1. (b). Calculated pressure differences across the X-rayed spot plotted against differences between pressures determined from the EOS of ruby and ice VII. Solid squares = compression; open circles = decompression. Curves = least-square fits of the compression data to a second-order polynomial (a) or a straight line (b).

ice-pressure determinations (Fig. 2b), indicating that this systematic difference probably results from the development of the pressure gradients and nonhydrostatic stresses; the estimated pressure gradient is, however, generally lower than the pressure discrepancies between the two pressure scales. A similar treatment of the ilmenite (012) and (104) line widths gives much lower pressure gradients across the X-ray beam (<0.3 GPa at the maximum pressure; this suggests that most of the line broadening is indeed due to the nonhydrostatic stresses that cause a larger line-width increase in ice than in ilmenite, not to an actual large pressure difference across the X-rayed zone. During decompression, the difference between the ruby and ice pressures becomes negative and the (110) ice line width increases further to a constant value of 240 eV; this effect may be partly due to an irreversible (e.g., plastic) deformation of the ice lattice or to a reduction of the grain size. Whatever the case, the pressure differences estimated from the ice line width are probably maximum values and may thus be regarded as uncertainties of the ice-pressure determ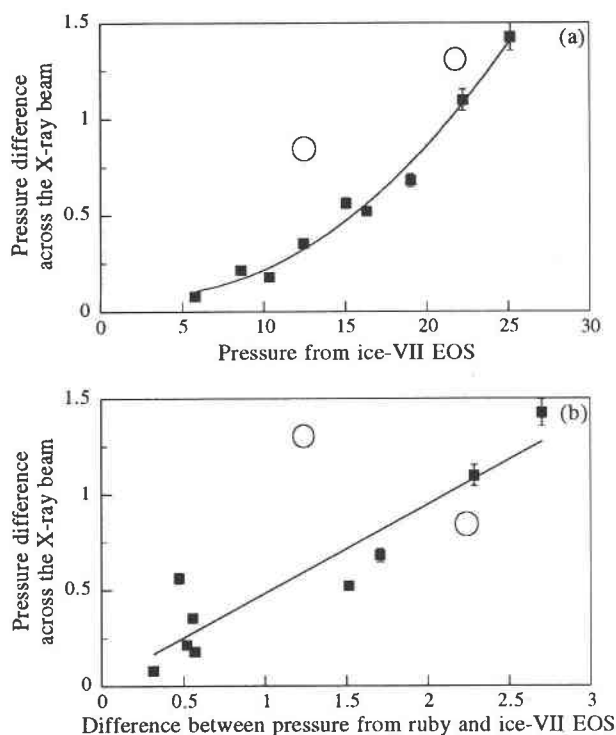inations. For reference, we will use the pressures determined from the ruby scale throughout the text, unless otherwise specified.

Lattice-parameter refinements and equation of state

The lattice parameters were calculated through a least-squares procedure with the assumption of hexagonal symmetry. Standard deviations were calculated for each parameter by using a constant reading uncertainty on peak positions (errors in geometry calibration, detector resolution) of ±60 eV (i.e., 10⁻² Å) and the standard deviation from least-squares fits of the peak position to Gaussian functions, which ranges from about 5 eV for the strongest bands to 70 eV for the weakest ones. Six to eight reflections were used to refine the parameters (Fig. 1, Table 1). Volumes were then fitted to third-order Eulerian finite-strain equations of state. The errors on the bulk modulus, K_0, and its pressure derivative, K_0', were calculated using the uncertainties in both the volume and pressure measurements.

RESULTS AND DISCUSSION

The unit-cell parameters of MgSiO₃ ilmenite as a function of pressure are given in Table 1. The ambient pressure pattern of the sample was first recorded in the dia-
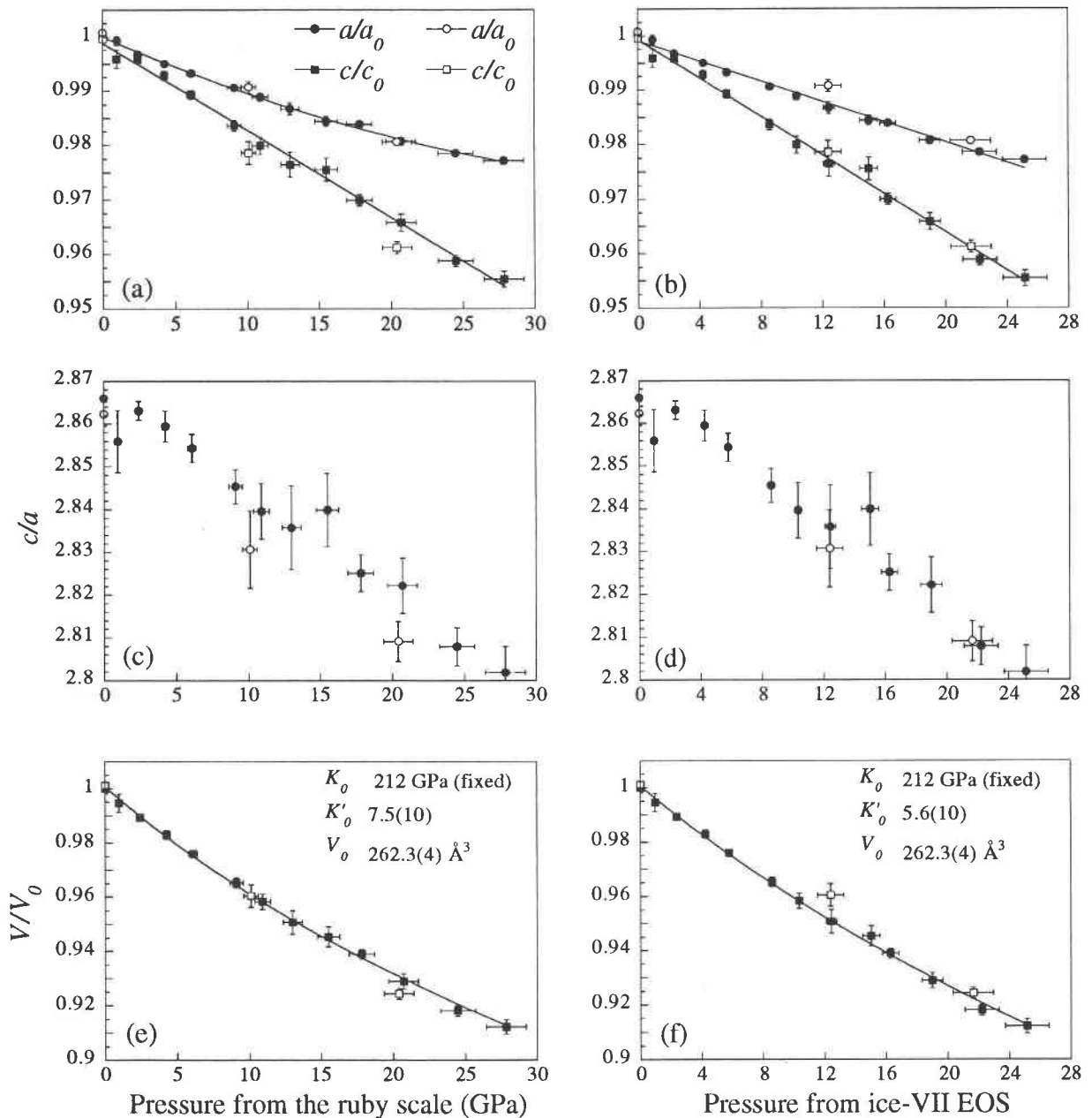
FIGURE 3. Evolution of the lattice parameters (**a** and **b**), c/a ratio (**c** and **d**), and cell volume (**e** and **f**) with pressure. Left = ruby-pressure scale; right = ice-VII–pressure scale. Solid symbols = compression data; open symbols = decompression data. Curves = fits of the compression data to polynomials (**a** and **b**) or to finite-strain equations of state (**e** and **f**).

mond-anvil cell to determine the reference volume. There is agreement within uncertainty between the ambient lattice parameters and our determination outside the high-pressure cell. There exists an ambiguity in the indexing of three observed reflections, which can correspond to (024) or (107), (116) or (205), (214) or (027), respectively. We chose to index these reflections as (024), (116), and (214) because this yields an ambient c/a ratio in better agreement with our determination outside the high-pressure cell and with previous determinations (Ito and Mat-

sui 1977) and reduces significantly the standard deviation on the cell parameters at high pressures.

The structure compresses anisotropically, with the c axis being nearly twice as compressible as the a axis (Figs. 3a and 3b; Table 2). This is a classical behavior for ilmenite structures at high pressures (Liu et al. 1974; Sato et al. 1977; Wechsler and Prewitt 1984; Ross et al., 1993) and contrasts with that of corundum-type structures in which the a and c axes have similar compressibility (Finger and Hazen 1978, 1980). The axial compression is

linear for the c axis and slightly curved for the a axis. This results in a c/a ratio that decreases slightly more at high pressures than at low pressures (Figs. 3c and 3d). This behavior can be understood by considering the different cation-cation interactions in the ilmenite structure. Compression along the c axis is achieved through a flattening of the $M^{2+}O_6$ octahedron, which is more compressible than the $M^{4+}O_6$ octahedron, causing a reduction in the M^{2+}-M^{4+} distances across face-sharing octahedra and M^{4+}-M^{4+} distances across a vacant site. On the other hand, compression of the a axis causes a reduction of the M^{2+}-M^{2+} and M^{4+}-M^{4+} distances across shared edges within the monocationic layer. The latter distances are less compressible in ilmenite (Wechsler and Prewitt 1984; Ross et al. 1993) because of the large M^{4+}-M^{4+} repulsion.

The 16 P-V data were used for the EOS determination, although upon decompression the points slightly fall off the fitted curves depending on which pressure scale is used; indeed, the refined parameters of the EOS are similar whether or not the decompression data are used. The ambient pressure volume was left to vary and never departed from our measurement in the cell by more than 0.01%. Because of the uncertainties associated with both the pressure and volume measurements, the refinement of both the bulk modulus and its pressure derivative yielded large uncertainties. Thus, we fixed the K_0 value at 212 GPa to check the consistency of our data with the Brillouin-scattering determination by Weidner and Ito (1985). If the ruby-pressure scale is used, fits of the P-V data yield $K'_0 = 7.5(10)$, whereas if the ice-pressure scale is used, $K'_0 = 5.6(10)$. We feel more confident in this latter value because the ice pressures were determined from the X-rayed area, and the value of 7.5 obtained for the ruby pressure is unrealistic for such a dense, close-packed structure as ilmenite. The fitted curves are consistent within errors bars with the P-V data, except for the decompression point near 10 GPa if the ice-pressure scale is used or for the decompression point near 20 GPa if the ruby scale is used; our measurements are thus consistent with the Brillouin-scattering data of Weidner and Ito (1985) and suggest that K'_0 is significantly larger than the value of 4 (second-order truncation of the Birch-Murnaghan EOS) commonly used to extrapolate ambient pressure determinations of K_0. Indeed, K'_0 higher than 4 have already been determined for close-packed structures such as Mg-rich silicate spinels (Hazen 1993; Rigden et al. 1991; Zerr et al. 1993).

The above conclusion implies that the ruby pressures are systematically overestimated in our experiment, except during decompression, leading to an overestimation of the elastic parameters. This overestimation is likely due to the pressure gradients and stresses, which increase with increasing pressure when a nonhydrostatic pressure-transmitting medium is used (Fig. 2b). However, it is unlikely that the ruby chips were at higher pressures than the X-rayed area because they were situated at the edges of the pressure chamber, which usually experience the lower pressures when pressure gradients develop. Thus,

TABLE 2. Axial compressibilities

P scale	Axis	β	β'	r^2
Ruby	a	−9.1(3)		0.9769
Ruby	a	−11.8(3)	13.1(15)	0.9970
Ruby	c	−16.8(2)		0.9968
Ice	a	−10.0(2)		0.9851
Ice	a	−12.3(3)	12.6(15)	0.9978
Ice	c	−18.2(2)		0.9974

Note: First- and second-order polynomial fits were weighted to an equation of the form $d/d_0 = 1 + \beta P + \beta' P^2$.

the overestimation of the ruby pressures with respect to the ice pressures may indeed be attributed to a specific effect of the nonhydrostatic stress on the position of the ruby-fluorescence line rather than to an actual pressure difference between the two measurement areas. A systematic overestimation of the ruby pressures in nonhydrostatic media may be invoked to reconcile the controversial compressibility data recently obtained on carbonates. The high-pressure, single-crystal diffraction studies of dolomite (Ross and Reeder 1992) and magnesite (Ross 1994) were performed in a 4:1 mixture of methanol and ethanol, which behaves hydrostatically within the investigated pressure ranges. They obtained bulk moduli of 94.1 and 117 GPa for dolomite and magnesite, respectively, which are in excellent agreement with single-crystal acoustic measurements of 94.9 (Humbert and Plicque 1972) and 112–113.8 GPa (Christensen 1972; Humbert and Plicque 1972). On the other hand, high-pressure powder diffraction data obtained using a nonhydrostatic medium yielded higher bulk moduli of 112.9 (Fiquet et al. 1994) and 137.5 GPa (Fiquet et al. 1994) for dolomite and magnesite, respectively, which are consistent with an overestimation of the ruby-scale pressures. This effect is probably more critical for carbonates than for MgSiO$_3$ ilmenite because of the larger compressibilities of carbonate phases.

REFERENCES CITED

Ashida, T., Kume, S., Ito, E., and Navrotsky, A. (1988) MgSiO$_3$ ilmenite: Heat capacity, thermal expansivity, and enthalpy of transformation. Physics and Chemistry of Minerals, 16, 239–245.

Christensen, N.I. (1972) Elastic properties of polycrystalline magnesium, iron, and manganese carbonates to 10 kilobars. Journal of Geophysical Research, 77, 369–372.

Fei, Y., Saxena, S.K., and Navrotsky, A. (1990) Internally consistent thermodynamic data and equilibrium phase relations for compounds in the system MgO-SiO$_2$ at high pressure and high temperature. Journal of Geophysical Research, 95, 6915–6928.

Finger, L.W., and Hazen, R.M. (1978) Crystal structure and compression of ruby to 46 kbar. Journal of Applied Physics, 49, 5823–5826.

——— (1980) Crystal structure and isothermal compression of Fe$_2$O$_3$, Cr$_2$O$_3$, and V$_2$O$_3$ to 50 kbar. Journal of Applied Physics, 51, 5362–5367.

Fiquet, G., Guyot, F., and Itié, J.-P. (1994) High-pressure X-ray diffraction study of carbonates: MgCO$_3$, CaMg(CO$_3$)$_2$, and CaCO$_3$. American Mineralogist, 79, 15–23.

Gasparik, T. (1990) Phase relations in the transition zone. Journal of Geophysical Research, 95, 15751–15769.

Hazen, R.M. (1993) Comparative compressibilities of silicate spinels: Amomalous behavior of (Mg,Fe)$_2$SiO$_4$. Science, 259, 206–209.

Hemley, R.J., Jephcoat, A.P., Mao, H.K., Zha, C.S., Finger, L.W., and Cox, D.E. (1987) Static compression of H_2O-ice to 128 GPa (1.28 Mbar). Nature, 330, 737–740.

Hogrefe, A., Rubie, D.C., Sharp, T.G., and Seifert, F. (1994) Metastability of enstatite in deep subducting lithosphere. Nature, 372, 351–353.

Humbert, P., and Plicque, F. (1972) Propriétés élastiques de carbonates rhomboédriques monocristallins: Calcite, magnésite, dolomite. Comptes Rendus de l'Académie des Sciences de Paris, 275, 391–394.

Ito, E., and Matsui, Y. (1977) Silicate ilmenites and the post-spinel transformations. In M.H. Manghnani and S. Akimoto, Eds., High-pressure research: Applications in geophysics, p. 193–208. Academic, New York.

Ito, E., and Yamada, H. (1982) Stability relations of silicate spinels ilmenites and perovskites. In S. Akimoto and M.H. Manghnani, Eds., High-pressure research in geophysics, 632 p. Center for Academic Publications, Tokyo, Japan.

Ito, E., and Navrotsky, A. (1985) MgSiO₃ ilmenite: Calorimetry, phase equilibria, and decomposition at atmospheric pressure. American Mineralogist, 70, 1020–1026.

Liu, L., Bassett, W.A., and Takahashi, T. (1974) Isothermal compression of a spinel phase of Co_2SiO_4 and magnesian ilmenite. Journal of Geophysical Research, 79, 1171–1174.

McMillan, P.F., and Ross, N.L. (1987) Heat capacity calculations for Al_2O_3 corundum and MgSiO₃ ilmenite. Physics and Chemistry of Minerals, 16, 225–234.

Neuville, D.R., and Richet, P. (1991) Viscosity and mixing in molten (Ca,Mg) pyroxenes and garnets. Geochimica et Cosmochimica Acta, 55, 1011–1019.

Rigden, S.M., Gwanmesia, G.D., Fitz Gerald, J.D., Jackson, I., and Liebermann, R.C. (1991) Spinel elasticity and structure of the transition zone of the mantle. Nature, 354, 143–145.

Ross, N.L. (1994) Magnesite at high pressure (abs.). Terra Nova, 6, 40.

Ross, N.L., and Reeder, R.J. (1992) High-pressure structural study of dolomite and ankerite. American Mineralogist, 77, 412–421.

Ross, N.L., Reynard, B., and Guyot, F. (1993) High-pressure structural study of MnGeO₃-ilmenite. Zeitschrift für Kristallographie, 204, 43–55.

Sato, Y., Ito, E., and Akimoto, S. (1977) Hydrostatic compression of ilmenite phase of ZnSiO₃ and MgGeO₃. Physics and Chemistry of Minerals, 2, 171–176.

Sawamoto, H. (1987) Phase diagram of MgSiO₃ at pressures up to 24 GPa and temperatures up to 2200°C: Phase stability and properties of tetragonal garnet. In M.H. Manghnani and Y. Syono, Eds., High-pressure research in mineral physics, p. 209–220. Terra Scientific, Tokyo, Japan.

Wechsler, B.A. and Prewitt, C.T. (1984) Crystal structure of ilmenite (FeTiO₃), at high temperature and at high pressure. American Mineralogist, 69, 176–185.

Weidner, D.J., and Ito, E. (1985) Elasticity of MgSiO₃ in the ilmenite phase. Physics of the Earth and Planetary Interiors, 40, 65–70.

Zerr, A., Reichmann, H., Euler, H., and Boehler, R. (1993) Hydrostatic compression of γ-(Mg₀.₆,Fe₀.₄)₂SiO₄ to 50.0 GPa. Physics and Chemistry of Minerals, 19, 507–509.